STRUCTURE, MORPHOLOGICAL, MAGNETIC AND OPTICAL PROPERTIES OF $Cu_xMg_{1-x}Fe_2O_4$ (x = 0, 0.5, 1) NANO FERRITES SYNTHESIZED BY CO-PRECIPITATION METHOD

Tran Van Chinh[1*], Nguyen Thi Hoai Phuong[1], Vu Thi Thu Ha[2], Phan Thanh Xuan[1], Phung Khac Nam Ho[1]

Abstract: *$Cu_xMg_{1-x}Fe_2O_4$ nanoparticles were successfully synthesized by co-precipitation. The samples were calcined at 900 ^oC for 3 h and X-ray diffraction analysis showed that $Cu_{0.5}Mg_{0.5}Fe_2O_4$ had a single phase cubic spinel structure, while formation of secondary phase of Fe_2O_3 was observed in XRD patterns of $CuFe_2O_4$, $MgFe_2O_4$. The saturation magnetization (M_s) of $Cu_{0.5}Mg_{0.5}Fe_2O_4$ is in between the saturation magnetization values of $CuFe_2O_4$ and $MgFe_2O_4$ nanoparticles, $CuFe_2O_4$ is a ferromagnetic material, while $MgFe_2O_4$ and $Cu_{0.5}Mg_{0.5}Fe_2O_4$ show superparamagnetic behavior. The synthesized spinel ferrites were fully characterized using scanning electron microscopy (SEM), FTIR spectroscopy, energy dispersive spectroscopy (EDS) and UV-vis spectrophotometry.*

Keywords: Spinel ferrites; Nanoparticles; Ferromagnetic materials; Superparamahnetic.

1. INTRODUCTION

Spinel ferrite nanoparticles have a general formula of MFe_2O_4, where M is a divalent metal cation such as Co^{2+}, Ni^{2+}, Cu^{2+}, Mg^{2+}, Zn^{2+}, Mn^{2+} are promising materials because of their unique magnetic and electric properties with chemical and thermal stabilities [1]. These materials have been used in many applications, including electrochemical supercapacitors [2], lithium-ion batteries [3], magnetic fluid hyperthermia [4], biomedical nanotechnology [5], drug delivery [6], gas sensors [7]. They have been routinely applied in wastewater treatment, in particular, in order to remove toxic metal [8, 9] and degrade organic dye [10, 11]. There are various methods for the synthesis of spinel ferrite such as co-precipitation [12], sol-gel [13], citrate-gel auto-combustion [14], ball-milling [15],…

Magnesium ferrite ($MgFe_2O_4$) is a soft magnetic n-type semiconductor with and a typical inverse spinel, where Fe^{3+} ions are located in the tetrahedral (A) and octahedral (B) sites and Mg^{2+} ions are only located in octahedral sites [16]. Copper ferrite ($CuFe_2O_4$) is basically an inverse of spinel ferrite and a high saturation field [17, 18].

In this work, the mixed cubic spinel ferrites nanoparticles $Cu_xMg_{1-x}Fe_2O_4$ (x = 0, 0.5, 1) were synthesized by the co-precipitation method. The structure, morphological, optical, and magnetic properties of these spinel ferrites are investigated

2. EXPERIMENTAL SECTION

Materials: Ferric chloride hexahydrate $FeCl_3{\cdot}6H_2O$ (98 %, Xilong-China), copper chloride hydrate $CuCl_2.2H_2O$ (99%, Xilong-China), magnesium chloride hydrate $MgCl_2{\cdot}6H_2O$ (99 %, Xilong-China), sodium hydroxide NaOH (99 %, Xilong-China), ethanol (99 %, Xilong-China), deionized water (D.I). All chemicals were used as such without any purification.

***Characterization techniques*:** Structure and crystallinity were analyzed by

X'Pert PRO PANalytical with a 0.15405 nm Cu-Kα radiation source. The morphology, particle size and elemental analysis of the samples were determined by a scanning electron microscope energy dispersive X-ray spectroscopy (SEM - EDX Hitachi S-4600). Fourier transform infrared spectroscopy (FTIR, TENSOR II, Bruker) was employed to investigate the surface functional group adsorbent of prepared nanostructured samples. Optical absorption spectra were measured by UV-vis spectrophotometer (Jasco V730). Magnetization measurements were carried out with a vibrating sample magnetometer (VSM) at room temperature.

Synthesis of $Cu_xMg_{1-x}Fe_2O_4$ (x= 0, 0.5, 1) nanoparticles: The $Cu_xMg_{1-x}Fe_2O_4$ (x=0, 0.5, 1) nanoparticles were prepared using a chemical co-precipitation method [19]. The molar ratio of M^{2+}/Fe^{3+} (M = Cu, Mg) was kept constant at 1:2. These materials in the stoichiometric ratio were dissolved in 100 ml deionized water and was vigorously stirred using a magnetic agitator for 15 minutes. A solution NaOH 5M was dropped to adjust the pH = (9 - 10). The precipitate was heated at 90 ^oC under magnetic stirring for 2 hours. After cooling, the solid materials were filtered and washed several times by D.I and ethanol. The washed samples were dried at 100 ^oC for 12 hours and then calcined at temperatures 900 ^oC for 3 hours.

3. RESULTS AND DISCUSSION

SEM analysis of the nanoparticles

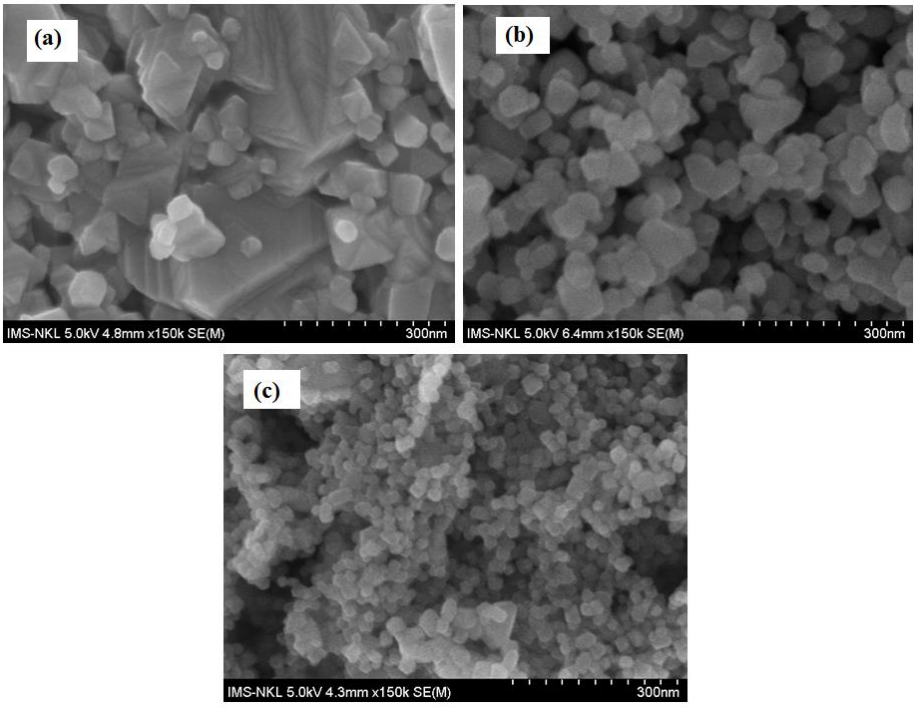

Figure 1. *SEM images of (a) $CuFe_2O_4$, (b) $MgFe_2O_4$ and (c) $Cu_{0.5}Mg_{0.5}Fe_2O_4$ nanoparticles.*

The morphologies of $CuFe_2O_4$, $MgFe_2O_4$ and $Cu_{0.5}Mg_{0.5}Fe_2O_4$ nanoparticles were studied by a scanning electron microscope (SEM) as shown in figure 1. The average size of $CuFe_2O_4$ nanoparticles is less than 100 nm with particle

aggregation into larger particles. The micrograph of $MgFe_2O_4$ has formed relative spherical particles with nano diameters in the range of 30 - 40 nm. And from fig 1c, the particles of $Cu_{0.5}Mg_{0.5}Fe_2O_4$ are relatively uniform in size with an average particle size of approximately 30 nm. The SEM observation of samples showed that the average size is in good agreement with their crystallite sizes determined from XRD spectra.

XRD analysis of the samples

XRD patterns of the $CuFe_2O_4$, $MgFe_2O_4$ and $Cu_{0.5}Mg_{0.5}Fe_2O_4$ nanoparticles were analyzed using XRD and shown in fig.2. As can be seen in fig.2**,** all the diffraction peaks at 19.05^o, 30.35^o, 35.08^o, 37.77^o, 43.97^o, 54.36^o, 58.4^o, 62.48^o, 65.09^o and 67.23^o, 74.25^o. The peaks correspond to the (111), (220), (311), (222), (400), (422), (511) (440), (531), (442) and (533) crystal planes, respectively, which are well matched with the standard diffraction pattern of spinel $CuFe_2O_4$ (JCPDS 01-077-0010) and spinel $MgFe_2O_4$ (JCPDS 01-089-3084). Moreover, the formation of the secondary phase of Fe_2O_3 (JCPDS 01-085-0599) was observed in XRD patterns of $CuFe_2O_4$, $MgFe_2O_4$. The secondary phase was also reported for other ferrites in literatures [20, 21]. While, the XRD pattern of $Cu_{0.5}Mg_{0.5}Fe_2O_4$ sample has only a single spinel phase with diffraction planes (200), (311), (400), (422), (511) and (440). Finally, these diffraction peaks of the $CuFe_2O_4$, $MgFe_2O_4$ and $Cu_{0.5}Mg_{0.5}Fe_2O_4$ are indexed to the cubic crystal structure of the spinel phase with the Fd-3m space group.

The crystallite size for the most intense peak (311) plane was calculated by using the Debye-Scherrer formula:

$$D = \frac{k.\lambda}{\mathrm{B}.\cos\theta}$$

Where *k*, λ, B and Θ are Scherrer constant (0.89), the X-ray wavelength (0.15406 nm), the width of the peak at half maximum intensity (radian) and the angle of diffraction, respectively [16].

The lattice parameter was also calculated from XRD data for all the samples using the equation:

$$a = \frac{\lambda.\sqrt{h^2 + k^2 + l^2}}{2.sin\theta}$$

Where (hkl) are Miller indices.

Table 1. *Crystallite size and lattice parameter for the samples.*

Samples	Crystallite size (nm)	Lattice parameter (Å)
$CuFe_2O_4$ (x = 1)	32.9	8.4836
$MgFe_2O_4$ (x = 0)	27.9	8.2785
$Cu_{0.5}Mg_{0.5}Fe_2O_4$ (x = 0.5)	29.5	8.2940

The crystallite size and the lattice parameter of the samples is shown in table 1.

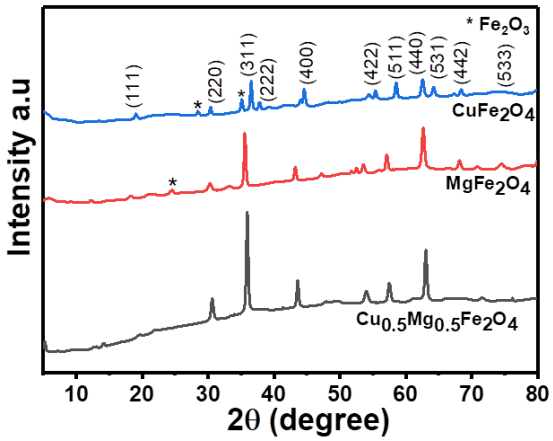

Figure 2. *XRD patterns of the $CuFe_2O_4$, $MgFe_2O_4$ and $Cu_{0.5}Mg_{0.5}Fe_2O_4$.*

The calculated lattice parameter for $MgFe_2O_4$ is smaller than the lattice parameter for $CuFe_2O_4$. This can be explained on the basis of ionic radius, where the ionic radius of Mg^{2+} ion (0.72 Å) [22] is smaller than that of Cu^{2+} ion (0.73 Å) [22]. When a larger Cu^{2+} ion is replaced by a smaller Mg^{2+} ion, the lattice parameter for $Cu_{0.5}Mg_{0.5}Fe_2O_4$ is smaller than the parameter for $CuFe_2O_4$ and larger than the parameter for $MgFe_2O_4$.

EDX analysis of the nanoparticles

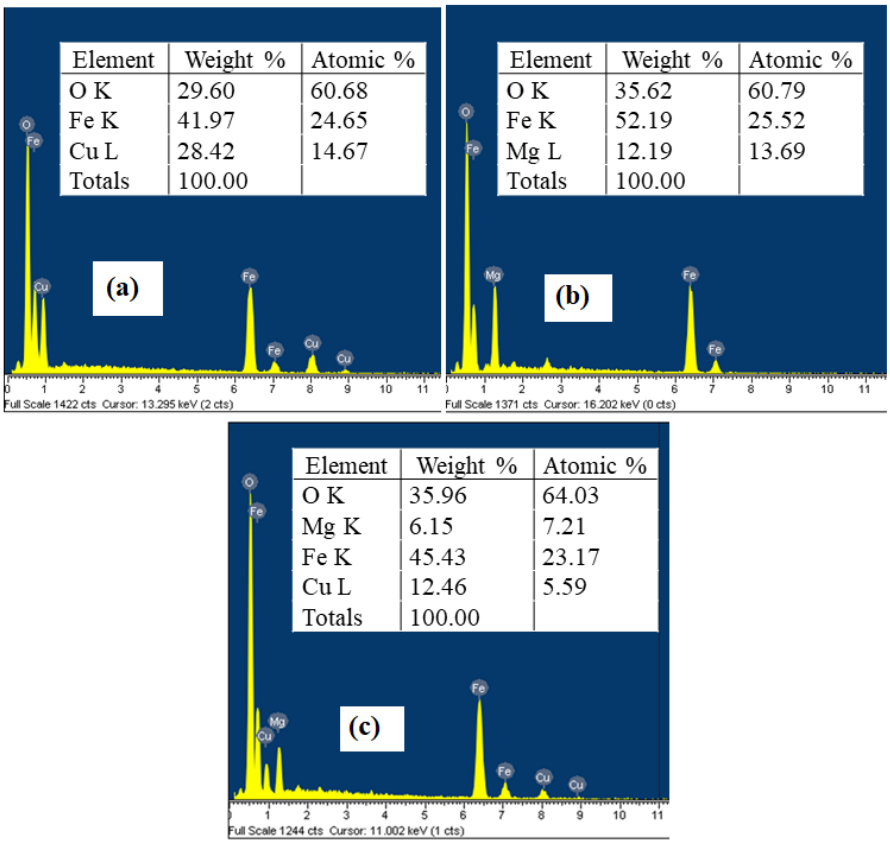

Figure 3. *EDX analysis of (a) $CuFe_2O_4$, (b) $MgFe_2O_4$ and (c) $Cu_{0.5}Mg_{0.5}Fe_2O_4$.*

Elemental analysis of $CuFe_2O_4$, $MgFe_2O_4$ and $Cu_{0.5}Mg_{0.5}Fe_2O_4$ samples based on EDX study (fig. 3). Fig. 3 shows the presence of peaks related to their constituent elements, with no other impurity. The Cu:Fe; Mg:Fe, and (Cu+Mg):Fe atomic ratios estimated by EDX analysis were (14.67:24.65), (13.69:25.52) and (12.8:23.17) which are nearly closeto the theoretical ratio of 1:2 in $CuFe_2O_4$, $MgFe_2O_4$ and $Cu_{0.5}Mg_{0.5}Fe_2O_4$, respectively.

FT-IR and Magnetization analysis of the nanoparticles

The Fourier transform infrared (FTIR) spectra of $CuFe_2O_4$, $MgFe_2O_4$ and $Cu_{0.5}Mg_{0.5}Fe_2O_4$ are presented in fig 4a. For three samples, the peaks around 3400 cm^{-1} and 1600 cm^{-1} are the contribution from the vibration of O-H group of adsorbed water or humidity on the surface [23, 24]. In the spinel ferrite structure, the metal ions are situated in two different sub-lattices designated as tetrahedral (A-site) and octahedral (B-site). The highest IR band ν_1, is generally observed in the higher frequency range of 600 - 550 cm^{-1}, corresponding to the intrinsic stretching vibration of the metal-oxygen bond at the tetrahedral site M_{tetra}-O (A-site). The lowest IR band ν_2, is usually observed in the frequency range of 450 - 385 cm^{-1}, assigned to stretching vibrations of the metal-oxygen bond at the octahedral site M_{octa}-O (B-site) [25, 26]. The values of ν_1 and ν_2 for samples are given in table 2 and confirm the formation of a spinel ferrite structure.

Table 2. *Absorption band (ν_1 and ν_2) of the samples.*

Samples	ν_1 (cm^{-1})	ν_2 (cm^{-1})
$CuFe_2O_4$ (x = 1)	583.11	434.24
$MgFe_2O_4$ (x = 0)	576.13	436.95
$Cu_{0.5}Mg_{0.5}Fe_2O_4$ (x = 0.5)	576.95	433.98

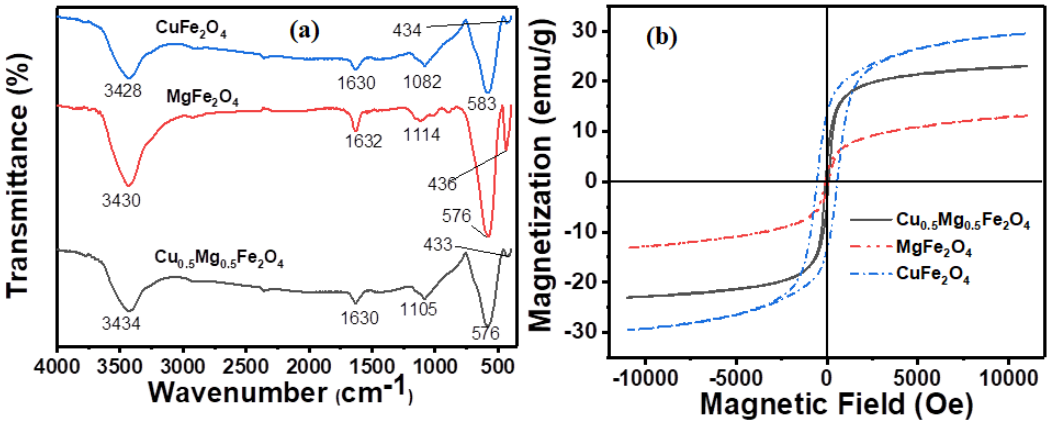

Figure 4. *(a) FTIR spectra and (b) Magnetic hysteresis loops of $CuFe_2O_4$, $MgFe_2O_4$, $Cu_{0.5}Mg_{0.5}Fe_2O_4$ nanoparticles.*

Hysteresis loops depicting the variation of magnetization (M, emu/g) and magnetic field (H, Oe) are shown in fig. 4b. The saturation magnetization (M_s), remanent magnetization (M_r) and coercivity (H_c) for all the samples are listed in the table 3**.** It was seen that the hysteresis loop of $CuFe_2O_4$ bears typical

characteristics of ferromagnetic materials, while $MgFe_2O_4$ and $Cu_{0.5}Mg_{0.5}Fe_2O_4$ show superparamagnetic behavior. The values of M_s, M_r, H_c of $CuFe_2O_4$ are higher than that of both $MgFe_2O_4$ and $Cu_{0.5}Mg_{0.5}Fe_2O_4$. The saturation magnetization of $MgFe_2O_4$ is exceptionally low, after replacing Mg^{2+} by Cu^{2+} to enhance the M_s value of $MgFe_2O_4$.

Table 3. *Saturation magnetization (M_s), remanent magnetization (M_r) and coercivity (H_c) of the samples.*

Samples	M_s (emu/g)	M_r (emu/g)	H_c (Oe)
$CuFe_2O_4$ (x = 1)	29.5	13.6	560
$MgFe_2O_4$ (x = 0)	13.1	1.6	83
$Cu_{0.5}Mg_{0.5}Fe_2O_4$ (x = 0.5)	23.1	4.1	83

Ultraviolet - visible analysis of the samples

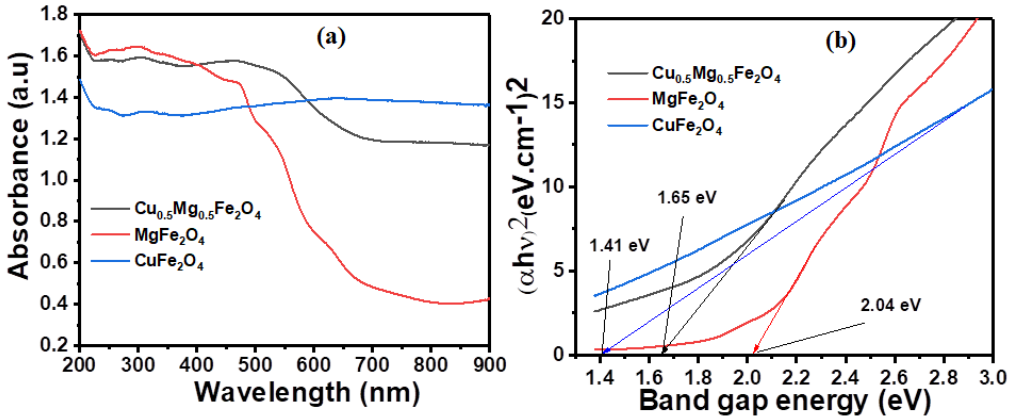

Figure 5. *(a) UV-vis absorption spectra and (b) Tauc plot of the $CuFe_2O_4$, $MgFe_2O_4$, $Cu_{0.5}Mg_{0.5}Fe_2O_4$ nanoparticles.*

The UV-vis absorption spectra of $CuFe_2O_4$, $MgFe_2O_4$ and $Cu_{0.5}Mg_{0.5}Fe_2O_4$ is shown in fig.6a. All the samples show a wide range of absorption from UV to visible region (200 nm - 850 nm). The optical absorption strength depends on the difference between the photon energy and the band gap as shown in the equation:

$$(\alpha h\upsilon)^{1/n} = A(h\upsilon - E_g)$$

where h is Planck's constant ($6{,}626.10^{-34}$ Js), υ is the light speed (3.10^8 ms^{-1}), α is the adsorption coefficient, E_g is the band gap energy and A is the absorption. The catalyst is assumed to be the direct transition type (n=1/2) for the determination of the band gap energy of the photocatalysts. By using the Tauc method, a plot $(\alpha h\upsilon)^2$ vs hυ was developed as shown in figure 5(b) and the calculated band gaps of energy are 1.41 eV, 2.04 eV, 1.65 eV for $CuFe_2O_4$, $MgFe_2O_4$, $Cu_{0.5}Mg_{0.5}Fe_2O_4$ respectively, indicating that the samples may have visible-light photoactivity.

4. CONCLUSIONS

In summary, $Cu_xMg_{1.x}Fe_2O_4$ (x = 1, 0.5, 0) nanoparticles were successfully synthesized by co-precipitation. At calcined 900 ^oC for 3 hours, $Cu_{0.5}Mg_{0.5}Fe_2O_4$

had a single phase cubic spinel structure, while $CuFe_2O_4$, $MgFe_2O_4$ had formation of secondary phase of Fe_2O_3 in XRD patterns. The particles sizes of $CuFe_2O_4$, $Cu_{0.5}Mg_{0.5}Fe_2O_4$ and $MgFe_2O_4$ were 32.9 nm, 27.9 nm and 29.5 nm, respestively. Cu^{2+}-doping improves the magnetic properties of magnesium ferrite, as the saturation magnetization (M_s) is increased from 13.1 emu/g to 23.1 emu/g. These spinel ferrites had small band gap energies of 1.41 eV, 2.04 eV, 1.65 eV for $CuFe_2O_4$, $MgFe_2O_4$, $Cu_{0.5}Mg_{0.5}Fe_2O_4$, respectively, indicating that they are used as adsorbents/photocatalysts for application in wastewater treatment.

Acknowledgement: The authors are grateful to the colleagues of the Department of Inorganic Chemistry, Institute of Chemistry and Materials.

REFERENCES

[1]. Maensiri, S., et al., "*A simple route to synthesize nickel ferrite ($NiFe_2O_4$) nanoparticles using egg white,"* Scripta materialia, **Vol. 56(9),** p. 797-800, (2007).

[2]. Reddy, A.E., et al., "*Construction of novel nanocomposite ZnO@ $CoFe_2$ O_4 microspheres grown on nickel foam for high performance electrochemical supercapacitors,"* Analytical Methods, **Vol. 10(2**), p. 223-229, (2018).

[3]. Popov, A.M., et al., *"Determination of lithium in lithium-ionic conductors by laser-enhanced ionization spectrometry with laser ablation,"* Journal of Analytical Atomic Spectrometry, **Vol. 29(1),** p. 176-184, (2014).

[4]. Céspedes, E., et al.,*"Bacterially synthesized ferrite nanoparticles for magnetic hyperthermia applications,"* Nanoscale, **Vol. 6(21)**, p. 12958-12970, (2014).

[5]. Srinivasan, S.Y., et al., *"Applications of cobalt ferrite nanoparticles in biomedical nanotechnology,"* Nanomedicine, **Vol. 13(10),** p. 1221-1238, (2018).

[6]. Yoon, T.J., et al., *"Multifunctional nanoparticles possessing a "magnetic motor effect" for drug or gene delivery,"* Angewandte Chemie, **Vol. 117(7),** p. 1092-1095, (2005).

[7]. 7. Šutka, A. and K.A. Gross, *"Spinel ferrite oxide semiconductor gas sensors,"* Sensors Actuators B: Chemical, **Vol. 222,** p. 95-105, (2016).

[8]. Salman, G., A. Bohan, and G. Jaed, *"Use of Nano-Magnetic Material for Removal of Heavy Metals from Wastewater,"* Engineering Technology Journal, **Vol. 35(9 Part (A) Engineering)**, p. 903-908, (2017).

[9]. Vamvakidis, K., et al., *"Diverse Surface Chemistry of Cobalt Ferrite Nanoparticles to Optimize Copper (II) Removal from Aqueous Media,"* Materials, **Vol. 13(7)**, p. 1537, (2020).

[10]. Abraham, A.G., et al., *"Enhanced magneto-optical and photo-catalytic properties of transition metal cobalt (Co^{2+} ions) doped spinel $MgFe_2O_4$ ferrite nanocomposites,"* Journal of Magnetism Magnetic Materials, **Vol. 452**, p. 380-388, (2018).

[11]. Ortiz-Quiñonez, J.-L., U. Pal, and M.S. Villanueva, *"Structural, magnetic, and catalytic evaluation of spinel Co, Ni, and Co–Ni ferrite nanoparticles fabricated by low-temperature solution combustion process,"* ACS omega, **Vol. 3(11),** p. 14986-15001, (2018).

[12]. Lassoued, A., et al., *"Synthesis and magnetic characterization of Spinel ferrites MFeO (M= Ni, Co, Zn and Cu) via chemical co-precipitation method,"* Journal of Materials Science: Materials in Electronics, **Vol. 28(24)**, (2017).

[13]. Bhandare, S.V., et al., *"Mechanistic insights into the sol-gel synthesis of complex (quaternary) Co–Mn–Zn-spinel ferrites: An annealing dependent study,"* Ceramics International, **Vol. 46(11),** p. 17400-17415, (2020).

[14]. Mohammad, A.M., S.M.A. Ridha, and T.H. Mubarak, *"Dielectric properties of Cr-substituted cobalt ferrite nanoparticles synthesis by citrate-gel auto combustion method,"* International Journal of Applied Engineering Research, **Vol. 13(8),** p. 6026-6035, (2018).

[15]. Bid, S. and S. Pradhan, *"Preparation of zinc ferrite by high-energy ball-milling and microstructure characterization by Rietveld's analysis,"* Materials Chemistry Physics, **Vol. 82(1)**, p. 27-37, (2003).

[16]. Nguyen, L.T., et al., *"A Facile Synthesis, Characterization, and Photocatalytic Activity of Magnesium Ferrite Nanoparticles via the Solution Combustion Method,"* Journal of Chemistry, **Vol. 2019**, (2019).

[17]. Kader, S.S., D.P. Paul, and S.M. Hoque, *"Effect of temperature on the structural and magnetic properties of $CuFe_2O_4$ nano particle prepared by chemical co-precipitation method,"* International Journal of Materials, Mechanics Manufacturing, **Vol. 2(1)**, p. 5-8, (2014).

[18]. Anandan, S., et al., *"Magnetic and catalytic properties of inverse spinel $CuFe_2O_4$ nanoparticles,"* Journal of Magnetism and Magnetic Materials, **Vol. 432,** p. 437-443, (2017).

[19]. Shih, Y.-J., et al., *"Synthesis of magnetically recoverable ferrite (MFe_2O_4, M Co, Ni and Fe)-supported TiO_2 photocatalysts for decolorization of methylene blue,"* Catalysis Communications, **Vol.72**, p. 127-132, (2015).

[20]. Zaki, H., S. Al-Heniti, and T. Elmosalami, *"Structural, magnetic and dielectric studies of copper substituted nano-crystalline spinel magnesium zinc ferrite,"* Journal of Alloys compounds, Vol. 633, p. 104-114, (2015).

[21]. Airimioaei, M., et al., *"Synthesis and functional properties of the $Ni_{1-x}Mn_xFe_2O_4$ ferrites,"* Journal of alloys compounds, **Vol. 509(31),** p. 8065-8072, (2011).

[22]. Shannon, R.D., *"Revised effective ionic radii and systematic studies of interatomic distances in halides and chalcogenides,"* Acta crystallographica section A: crystal physics, diffraction, theoretical general crystallography, **Vol. 32(5),** p. 751-767, (1976).

[23]. Nguyen, T.B. and R.-a.J.R.A. Doong, *"Heterostructured $ZnFe_2$ O_4/TiO_2 nanocomposites with a highly recyclable visible-light-response for bisphenol A degradation,"* RSC Adv, **Vol. 7(79),** p. 50006-50016 (2016).

[24]. Manimozhi, V., et al., *"Preparation and characterization of ferrite nanoparticles for the treatment of industrial waste water,"* Digest Journal of Nanomaterials and Biostructures, **Vol. 11(3)**, p. 1017-1027, (2016).

[25]. Sezgin, N., et al., *"Synthesis, characterization and, the heavy metal removal efficiency of MFe_2O_4 (M= Ni, Cu) nanoparticles,"* Ekoloji, **Vol. 22(89),** p. 89-96, (2013).

[26]. Raju, M.K.J.C.S.T., *"FT-IR studies of Cu substituted Ni-Zn ferrites for structural and vibrational investigations,"* Chemical Science Transactions, **Vol. 4(1),** p. 137-142, (2015).

TÓM TẮT

CẤU TRÚC, HÌNH THÁI HỌC, TỪ TÍNH VÀ TÍNH CHẤT QUANG CỦA NANO FERRITE $Cu_xMg_{1-x}Fe_2O_4$ (x = 0, 0.5, 1) TỔNG HỢP BẰNG PHƯƠNG PHÁP ĐỒNG KẾT TỦA

Các hạt nano $Cu_xMg_{1-x}Fe_2O_4$ đã được tổng hợp thành công bằng phương pháp đồng kết tủa. Các mẫu được nung ở 900 ^oC trong 3 giờ, theo phổ XRD mẫu $Cu_{0.5}Mg_{0.5}Fe_2O_4$ có cấu trúc đơn pha dạng lập phương, trong khi đó, mẫu $CuFe_2O_4$ và $MgFe_2O_4$ có sự xuất hiện của pha Fe_2O_3. Từ độ bão hòa của $Cu_{0.5}Mg_{0.5}Fe_2O_4$ nằm trong khoảng giữa giá trị từ độ bão hòa của $CuFe_2O_4$ và $MgFe_2O_4$. $CuFe_2O_4$ là vật liệu sắt từ, $Cu_{0.5}Mg_{0.5}Fe_2O_4$ và $MgFe_2O_4$ là vật liệu siêu thuận từ. Tất cả các spinel ferrite được đánh giá một số tính chất như SEM, FT-IR, EDS và phổ UV-vis.

Từ khóa: Spinel ferrite; Hạt nano; Vật liệu sắt từ; Siêu thuận từ.

Received Jan 11th 2021
Revised Jan 26th 2021
Published May 10th 2021

Author affiliations:
[1] Institute of Chemistry and Materials;
[2] Key Laboratory for Petrochemical and Refinery Technologies.
*Corresponding author: chinhpkkq@gmail.com.